School of Natural Sciences and Mathematics
William B. Hanson Center for Space Sciences

Modeling the Daytime Energy Balance of the Topside Ionosphere at Middle Latitudes

UT Dallas Author(s):

Chih-Te Hsu
Roderick A. Heelis

Citation:

Hsu, Chih-Te, and Roderick A. Heelis. 2017. "Modeling the daytime energy balance of the topside ionosphere at middle latitudes." Journal of Geophysical Research-Space Physics 122(5): 5733-5742.

AGU PUBLICATIONS

JGR

Journal of Geophysical Research: Space Physics

RESEARCH ARTICLE

10.1002/2017JA024112

Key Points:
- Dependence of ion temperature on ion composition agrees with observations
- O^+ heated by electrons and H^+
- H^+ cooled by collisions with O^+ and conduction

Correspondence to:
C.-T. Hsu,
chih-te.hsu@utdallas.edu;
heelis@utdallas.edu

Citation:
Hsu, C.-T., and R. A. Heelis (2017), Modeling the daytime energy balance of the topside ionosphere at middle latitudes, *J. Geophys. Res. Space Physics*, *122*, 5733–5742, doi:10.1002/2017JA024112.

Received 2 MAR 2017
Accepted 6 MAY 2017
Accepted article online 10 MAY 2017
Published online 24 MAY 2017

Modeling the daytime energy balance of the topside ionosphere at middle latitudes

Chih-Te Hsu[1] **and Roderick A. Heelis**[1]

[1]William B. Hanson Center for Space Sciences, University of Texas at Dallas, Richardson, Texas, USA

Abstract Recently reported measurements from the Defense Meteorological Satellite Program (DMSP) indicate that the O^+ temperature in the topside ionosphere is dependent on the fractional H^+ density. This finding indicates that the mass-dependent energy exchange rate between O^+ and H^+ plays an important role in the thermal balance of the topside ionosphere. In this study we utilize the SAMI2 model to retrieve both T_{H+} and T_{O+} and verify the previously observed dependence of ion temperature on ion composition. The model shows that in the topside at middle latitudes when a single ion is dominant, O^+ or H^+ is heated by electron collisions and cooled by conduction as expected. However, in the intervening altitude region where both O^+ and H^+ are present, O^+ is heated by collisions with H^+ and cooled by conduction, while H^+ is heated by collisions with electrons and cooled by collisions with O^+.

1. Introduction

The plasma temperatures in the topside ionosphere are determined by photoelectron heating, conduction, and collisional energy exchange between the ions and electrons [*Brace and Theis*, 1978; *Schunk and Nagy*, 1978]. During the daytime the thermal electrons are heated by photoelectrons that are created by photoionization of the neutral gas in the thermosphere and stream along magnetic flux tubes. The thermal electrons are cooled by collisions with ions and conduction. In a simple assumption that all ions have the same temperature, the ions are heated by collisions with electrons and cooled by conduction to lower altitudes where heat is lost through collisions with the neutral gas. During the nighttime, when the source of photoionization is absent, both ions and electrons are cooled by conduction to lower altitudes where heat is lost to the neutral gas [*Banks and Kockarts*, 1973].

Observations of ion and electron temperature retrieved from satellite measurements and incoherent scatter radar have provided a more complete description of the energy balance in the ionosphere. A daytime negative correlation between the total plasma density and electron temperature, which is generally attributed to the balance between photoelectron heating and collisional cooling, has been studied frequently [*Bailey et al.*, 2000; *Brace and Theis*, 1978; *Bilitza et al.*, 2007; *Kakinami et al.*, 2011] and also often used to synthesize empirical models and interpret first-principle model results [*Bilitza*, 1975; *Wang et al.*, 2006; *Zhang et al.*, 2004]. On the other hand, ions behave as intermediaries between the hot electrons and the cold neutral atmosphere revealing a positive correlation between N_i and T_i in the daytime topside ionosphere [*Banks*, 1967; *Titheridge*, 1998; *Kakinami et al.*, 2014]. The aforementioned discussion applies well to the ionosphere when a single ion species dominated the topside ionosphere. However, recent observations of the electron and ion temperature distribution at middle latitudes in the daytime [*Hsu and Heelis*, 2017] suggest that the O^+ temperature is larger in the presence of a H^+ dominant plasma than when O^+ is itself dominant. This exposes the role of H^+ in transferring heat from the electrons to the O^+ and the requirement to separately understand the heat transfer processes in each of the ion species. Many theoretical models incorporate the physical processes described above, which determine the electron temperature and the constituent ion temperature [*Millward et al.*, 1996; *Richards et al.*, 2009; *Richmond et al.*, 1992; *Qian et al.*, 2014]. Such models provide adequate descriptions of the diurnal and seasonal variations in the electron temperature [*Fallen and Watkins*, 2013; *Su et al.*, 1998]. However, recent studies of the constituent ion temperatures remain scarce [*Klimenko et al.*, 2008].

The SAMI2 (Sami2 is Another Model of the Ionosphere) developed by the Naval Research Laboratory is capable of investigating the energetics and dynamics of the low-latitude to midlatitude ionosphere [*Huba et al.*, 2000] in this way. The model has received extensive use and has shown agreement between the field-aligned ion drifts and the h_mF_2 at low latitudes [*Burrell and Heelis*, 2012] and succeeded in modeling the Weddell Sea anomaly [*Chen et al.*, 2011]. The electron temperature and the effects of conjugate photoelectron heating have also been investigated [*Chao et al.*, 2010; *Wu et al.*, 2012]. The model values have also been used to compare with C/NOFS satellite measurements in the extreme solar minimum periods [*Klenzing et al.*, 2013]. More recently, the plasma density profiles and the light-ion composition at Jicamarca have been modeled by using the improved version SAMI2-PE model [*Hysell et al.*, 2015]. In this paper, we use the model to aid in further interpretation of ion temperature measurement observed to be dependent on the ion composition.

2. Electron and Ion Temperature Observed by Defense Meteorological Satellite Program Satellite

The Defense Meteorological Satellite Program (DMSP) satellite F15 has an 840 km Sun-synchronous circular orbit and has been operated from 1999. It has been used to investigate the energy balance in the 0600–1100 LT sector from 30° to 50° magnetic latitude for the period 2004–2006 [*Hsu and Heelis*, 2017]. The F15 satellite is equipped with a Langmuir probe to measure electron temperature and a retarding potential analyzer to obtain current-voltage curves for derivation of the ion temperature, ion composition, and ram ion drift [*Heelis and Hanson*, 1998]. This allows an examination of the electron and ion temperatures, which are influenced by the heat exchanged between the different constituent ions and their dependencies on solar zenith angle, solar activity, and the relative abundance of O^+ and H^+.

The DMSP satellite is in a circular Sun-synchronous orbit. Thus, in the postsunrise middle latitude sector sampled by the DMSP satellite, variations in the plasma number density and the electron heating rate are driven primarily by changes in solar zenith angle produced by changes in season according to a standard Chapman production function derived by *Chapman* [1931]. In Figure 1, adapted from *Hsu and Heelis* [2017], the blue curves and accompanying deviations show the DMSP observations of electron temperature, the O^+ temperature, T_e-T_{O+}, and the H^+ fraction as a function of the plasma density at middle latitudes between 30° and 50° in the local time region between 0700 and 1100 obtained during the period 2004–2006. The overall plasma density increases as the solar zenith angle decreases with changes of season from winter to summer, while the electron temperature decreases as the plasma density increases due to the balance between the attenuated electron heating rate from the peak to the observation point and the electron cooling rate.

The variation in ion temperature also depends on changes in solar zenith angle, which control the plasma number density. The ion temperature increases to approach the electron temperature as the plasma density increases. This behavior reflects the local collisional heating of the ions by the electrons and the remote influence of conductive cooling to the neutrals. The additional influence at larger solar zenith angles may produce adiabatic cooling of the ions as they flow upward to fill the larger volume magnetic flux tubes in this postsunrise sector.

Hsu and Heelis [2017] also point out that the ion temperature is strongly dependent on the H^+ fraction such that within the variability shown, the highest O^+ temperatures correspond to the highest H^+ fractional content. This significant attribute of the DMSP observations may be understood by recognizing that the energy exchange between the electrons and ions is inversely proportional to the mass and thus the electrons preferentially heat the H^+ when it is present. However, the observations do not provide an independent measure of T_{H+} and T_{O+} so that the heat exchange processes for each of these species cannot be directly assessed. We utilize the SAMI2 model to verify the observed behavior and to examine the details of the energy balance in these circumstances.

3. Model

Here model values of T_e, T_i, and constituent ion density are computed using SAMI2 [*Huba et al.*, 2000]. The model solves coupled time-dependent equations of continuity, momentum, and temperature for different ions and the electrons along closed dipole magnetic field lines between base altitudes of about 85 km in conjugate hemispheres. It provides values for the concentrations, magnetic field-aligned velocity, and temperatures of the ions and electrons at a discrete set of points along the field lines. In the present study, the model equations are solved along 60 field lines assuming an eccentric dipole with apex heights ranging from 150 to 18,000 km altitude in approximately the same meridian plane. Each field line contains 101 grid points. The grid points are more closely spaced in altitude at low altitudes and more spread in altitude at high altitudes.

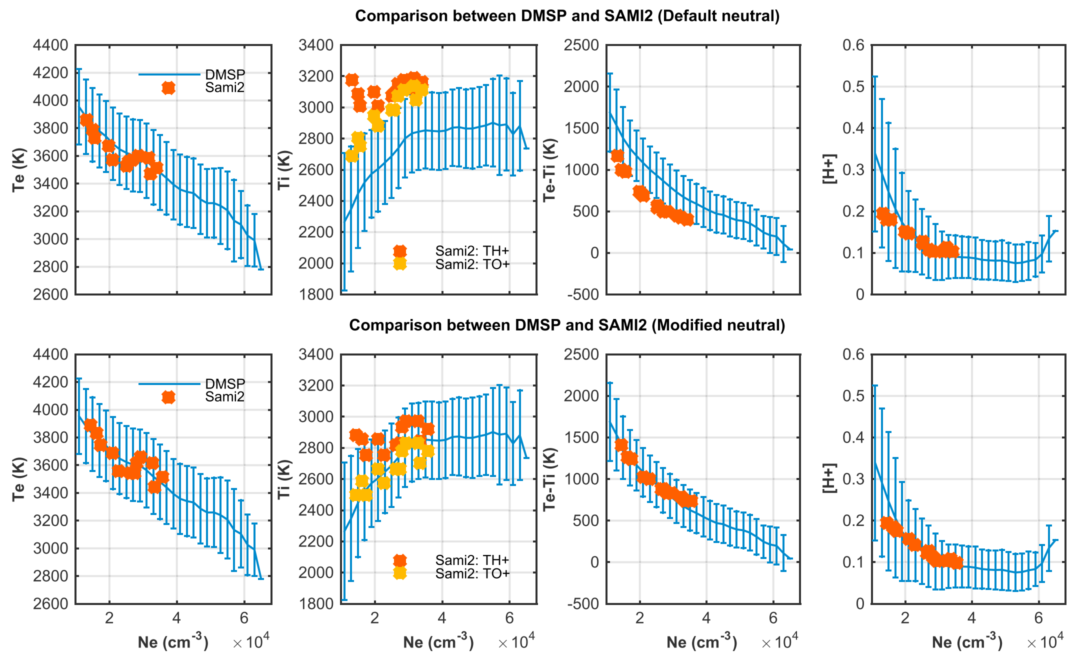

Figure 1. Comparison between SAMI2 model results and average DMSP measurements for the dependence of the electron temperature (T_e), ion temperature (T_i), T_e-T_i, and H^+ fraction ($[H^+]$) on the electron number density (N_e) at 0900 h local time at 840 km. The SAMI2 model results are indicated by colored dots and DMSP observations with their standard deviation by the blue traces. Results are shown (top row) for a standard (default) neutral atmosphere altitude profile and (bottom row) for an adjusted neutral atmosphere altitude profile. See text for details.

To understand the energy balance between electrons and different ions in the topside ionosphere, we choose the magnetic meridian located at 130° geographic longitude and 9.5° geographic latitude. At this location the magnetic meridian plane is almost parallel to geographic meridian plane, and all points on the magnetic flux tubes are approximately at the same local time. To simplify the calculations, a SAMI2 provided option to only consider the dominant ions in the ionosphere (H^+, O^+, NO^+, and $O_2{}^+$) is exercised. The thermal balance equations are solved for H^+, O^+, and the electrons with the temperature for molecular ions assumed to be the same as T_{O+}.

The starting time of the model run for each day is 1600 LT at the magnetic apex point. The model is initialized with a prerun of 24 h to insure that the model has reached a stable condition and results are subsequently recorded every 15 min for the next 24 model hours. The model time step is automatically self-adjusted to meet the Courant condition [*Huba et al.*, 2000] for all grid points and has a maximum limit of 30 s. We examine results for day 21 in every month of model year 2005 to approximate the conditions prevailing for the observations of DMSP from 2004 to 2006 reported earlier by *Hsu and Heelis* [2017]. Day 21 is chosen to give an equal distribution of points between the solstices.

In order to approximate the behavior of the satellite observations, the model results are taken at 840 km altitude, and in the rest of our study only the Northern Hemisphere is considered. A discrepancy between the satellite data and the model can be expected. The model results are extracted for the same altitude but for only one longitude, and the range of thermal processes, which are dependent on different geographic locations, on a particular flux tube is relatively small. The observations are at almost a fixed altitude, and averages in magnetic latitude between 30° and 50° and from all longitudes are ordered by solar zenith angle. This produces a wider range in the plasma density and temperature associated with various transport and chemistry effects and thus produces larger variations in plasma heating and cooling processes than exist in the models runs. However, it should be emphasized that it is not our intent to quantitatively reproduce the observations in the model. Rather, the general behavior of the plasma temperatures with respect to variations in the ionospheric parameters is more important. By selecting the solar activity level and associated neutral atmosphere, we can make the variation of the plasma temperature and density in the model reflect the major features of the average observations. In this way the underlying influences of the major heating and cooling processes can be revealed.

The SAMI2 calculates the neutral atmosphere constituent densities and neutral temperature from the MSISE model [*Picone et al*., 2002] and the neutral wind velocity from the HWM93 model [*Hedin et al*., 1996]. The $F_{10.7}$ solar flux index is the input parameter for these two models, producing larger topside neutral density under higher $F_{10.7}$ conditions. This $F_{10.7}$ index and its 81 day running average are also used to calculate the ionization rate based on the EUVAC model, which linearly scales a reference spectrum [*Richards et al*., 1994], resulting in a larger plasma production rate in the SAMI2 calculation under high $F_{10.7}$ conditions.

Various levels of sophistication can be applied to determine the photoelectron heating rate [*Varney et al*., 2012]. However, for our purposes we wish only to determine the relationships between the topside ionospheric density, composition, and the constituent species temperatures, to be compared with the observations made by the DMSP satellite. To accomplish this task, we utilize the formulations provided in the SAMI2 model, which scales the peak photoelectron heating rate by the peak ionization production rate and attenuates the heating rate above the peak by a factor proportional to the plasma column content. We choose the $F_{10.7}$ index to be 85 as representative of the mean condition under which the observations are made and adjust the photoelectron heating rate above the peak to best represent the electron temperature that is observed. We then compare the model ionospheric density and composition and ion temperatures to the observations.

4. Model Temperatures and Comparison With the Observation

The DMSP observation shows that the major parameters influencing the thermal energy balance in the topside ionosphere are the plasma density, ion composition, and electron temperature. For observations made at nearly constant altitude and local time the evolution of these ionospheric properties is driven by changes in solar zenith angle corresponding to changes in day of the year. Added to Figure 1 are the variations in electron temperature, ion temperature, and H^+ fractional content extracted from the model by selecting the data near 840 km at 40° magnetic latitude in the Northern Hemisphere. These model results are constructed every 21 days throughout the year, with those at the largest plasma densities occurring in northern summer and those with the smallest plasma densities occurring in northern winter.

Figure 1 (top row) shows the comparison between DMSP observations and SAMI2 results with no adjustments to the neutral atmosphere. The model results are in accord with the expected dependencies of temperature on density and indeed show that the H^+ temperature exceeds the O^+ temperature by 200 K as expected. However, the most significant departures are seen in determination of the O^+ temperature for which the model calculations consistently compute a value that is higher than that observed by 300–500 K. This is attributed to the neutral atmosphere composition and temperature specified by the empirical model which provides insufficient thermal contact with the neutral gas above the *F* peak.

At 840 km the ion temperature is determined primarily by the flow of heat from electrons to ions and is balanced by the flow of heat from the ions to the neutral gas, which is controlled by the integrated effect of collisional cooling to the neutrals in the region below. This cooling rate depends on the neutral densities along magnetic flux tubes and is characterized by the neutral scale height specified by the neutral temperature. In addition, the model H^+ concentration remains lower than is observed indicating that the neutral atmosphere composition in terms of the neutral atomic oxygen and hydrogen densities would need adjustment.

Since SAMI2 accesses the neutral model in a modular fashion, it is possible to adjust the plasma temperatures by changing the neutral density and photoelectron heating rate. To increase the thermal contact between the ions and the neutral gas in the topside, while leaving the lower ionosphere unchanged, we increase the exospheric temperature and the neutral hydrogen density. To compensate for the increasing energy sink of the neutral gas, we also increase the peak photoelectron heating rate by 20% to ensure that the electron temperature remains near the observed values.

The vertical profiles at 40° magnetic latitude in Figure 2 show a comparison between the originally specified neutral mass density, neutral temperature, O^+ temperature, and electron temperature and the modified output of these parameters for two model days corresponding to winter (top) and summer (bottom). The increase in exospheric temperature increases the topside neutral scale height producing higher neutral density at higher altitude. This raises the altitude at which the ion temperature transitions to the electron

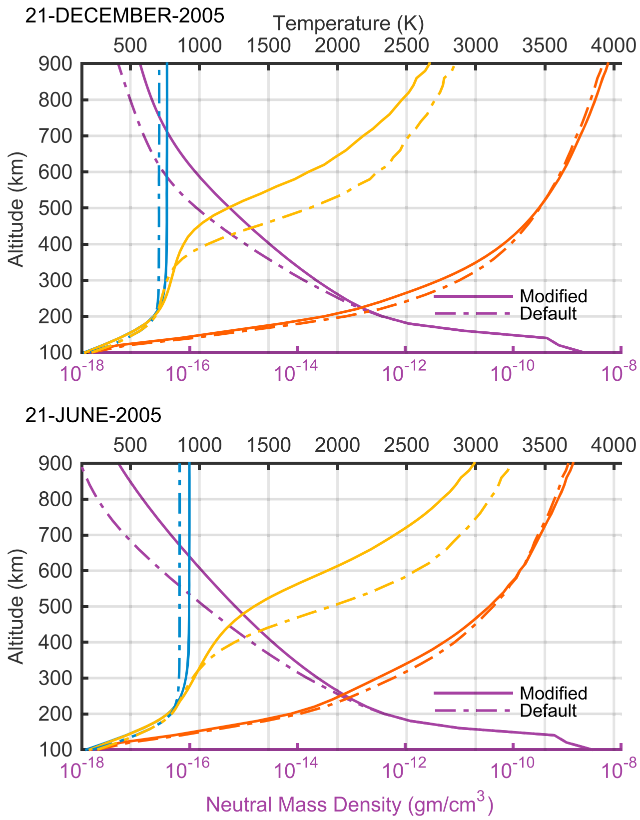

Figure 2. Standard (default) and adjusted altitude profiles of neutral mass density (purple) and temperature (blue) as well as ion (yellow) and electron (red) temperature at 0900 h local time for (top) winter and (bottom) summer.

temperature. The increased neutral scale height increases the topside neutral oxygen and enhances the topside helium concentration in the winter hemisphere. Figure 1 (bottom row) compares the observations of *Hsu and Heelis* [2017] with the values retrieved from the model with the modified neutral atmosphere. By implementing the modifications discussed above, the O^+ temperature at 840 km decreases by 300–500 K as required to approximate the observations.

After the modifications, we still see that in the presence of H^+ and O^+, the H^+ temperature is larger than the O^+ temperature. This also implies that the O^+ experiences two heat sources from collisions with the electrons and collisions with the lighter H^+ ions. We have also noted earlier that *Hsu and Heelis* [2017] have shown that for a fixed plasma density associated with a given solar zenith angle, the O^+ temperature is larger when

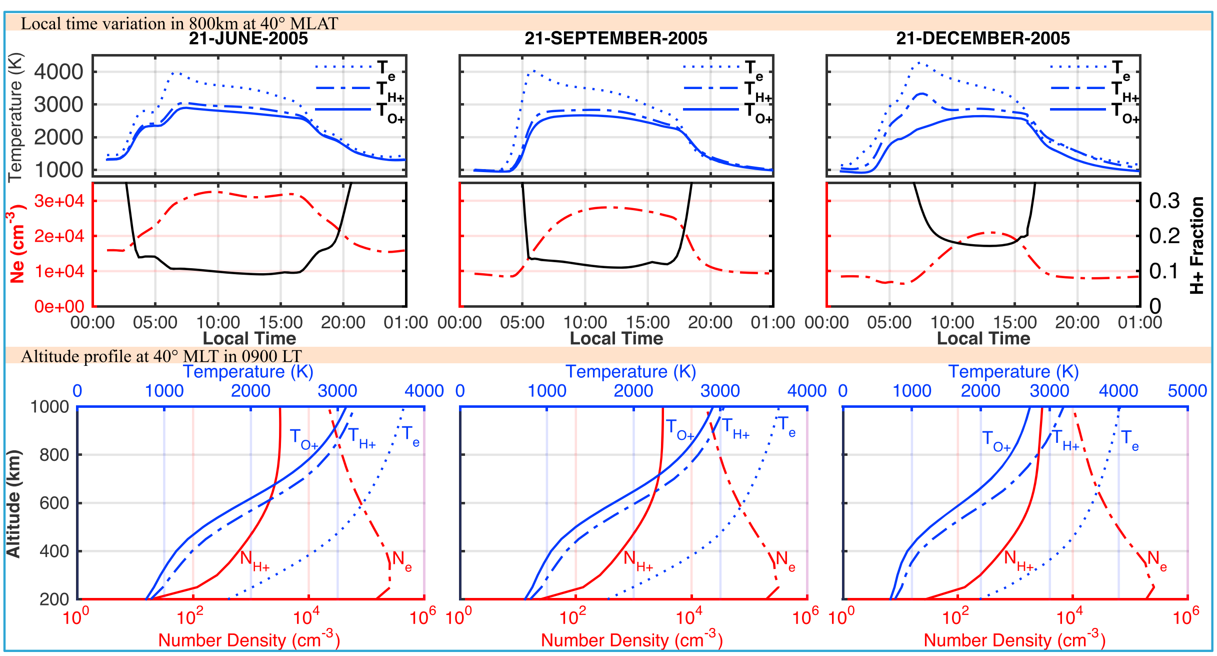

Figure 3. (top row) Plasma temperatures, plasma number density, and H^+ fraction as a function of local time at 40° magnetic latitude in 840 km. (bottom row) Altitude profiles of the same parameters at 0900 h local time.

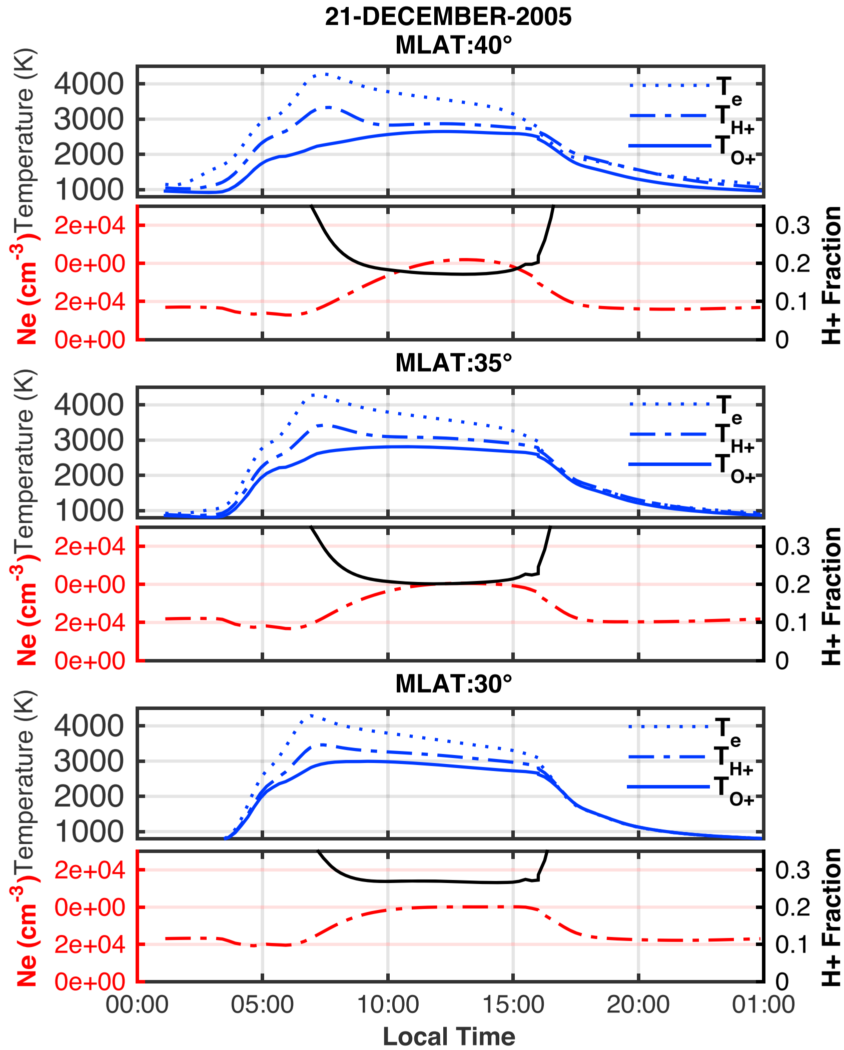

Figure 4. The plasma temperatures, plasma number density, and H^+ fraction as a function of local time from SAMI2 in 840 km for 40°, 35°, and 30° magnetic latitude.

the H^+ fractional content is larger. Having established a baseline model that reproduces the average variations in plasma density and temperature, we are now well positioned to describe the individual heating and cooling processes that give rise to the observed behavior.

5. Details of the Energy Balance

Further insights into the processes determining the ion and electron temperatures may be obtained by examining the ionospheric parameters and the individual heating and cooling terms as a function of local time and altitude. Figure 3 (top row) shows model plasma temperatures, plasma number density, and fractional H^+ density as a function of local time at 40° magnetic latitude and a fixed altitude of 840 km for three example days covering different seasons representative of the solstices and equinox. In Figure 3 (bottom row) is shown the altitude variation of these key parameters at 0900 local time. In space and time, the plasma density shows the typical daily variation that correlates with ionization production in the ionosphere and decreases with increasing altitude. Both the plasma density and the H^+ fraction are also in accord with the expected dependence on season. The topside plasma density is higher in the summer and lower in the winter, and the fractional H^+ contribution is lower in the summer compared to the winter.

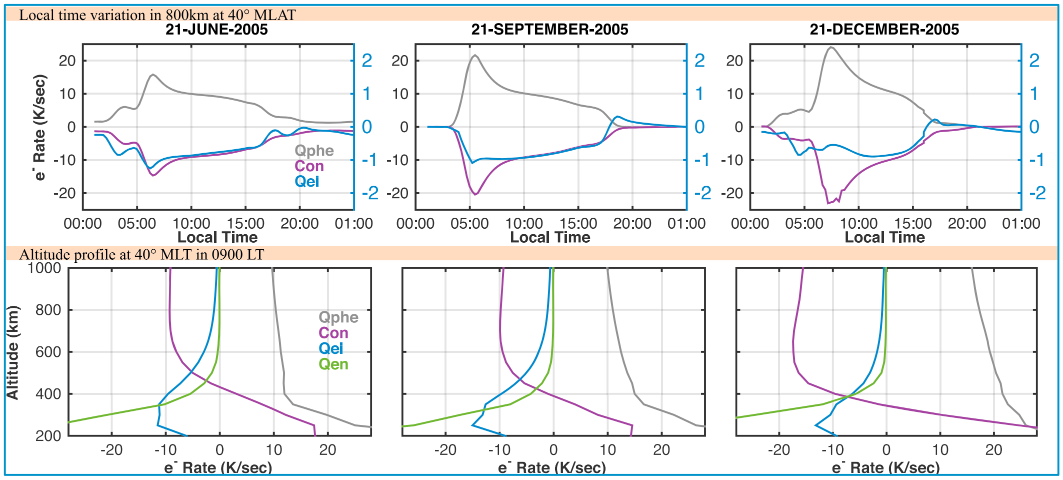

Figure 5. Model values of the major electron heating and cooling rates. (top row) Photoelectron heating (Q_{phe}), electron thermal conduction (Con), and total electron-ion collisional energy exchange (Q_{ei}) are shown as a function of local time at 40° magnetic latitude in 840 km. Note that the collisional cooling rate is specified by the scale to the right in each panel. (bottom row) Altitude profiles of the same parameters with additional electron-neutral collisional cooling (Q_{en}) at 0900 h local time.

By inspecting the local time changes, after sunrise we find that the electron temperature rises rapidly then decreases as the local time increases. Over the same time period, ions warm in response to the increased electron temperature, but a large temperature difference between the O^+ and electron temperature is present. Throughout the daytime, T_{H+} is generally higher than T_{O+} especially in the winter when the H^+ concentration is relatively higher and T_{H+} behaves more like T_e. Differences in the O^+ and H^+ temperatures exist in the daytime and may become substantial when the relative H^+ concentration is greater than 20%. In the winter midlatitudes we find conditions where the electron and O^+ temperatures differ by almost 2000 K while T_{O+} and T_{H+} differ by about 1000 K.

We have previously noted that the observations suggest that for the same solar zenith angle and the same plasma density, the O^+ temperature is larger when the H^+ fractional content is large. This may be verified in the model by examining the O^+ temperature for the same day at different latitudes. Figure 4 shows model plasma temperatures, plasma number density, and fractional H^+ density as a function of local time at a fixed altitude of 840 km in winter solstice for three different magnetic latitudes. We find that at a given local time during the daytime (e.g., 1000 LT) the total plasma density is almost the same. However, in the lower latitude region the O^+ temperature is higher when the H^+ fraction is larger as is reflected in the observations.

Figure 5 shows the variation of the electron heating and cooling terms with local time (top row) and altitude (lower row). The major contributions from photoelectron heating, conduction, and collisions are indicated in the first panel in each row. After sunrise the photoelectron heating rate rises rapidly as does the electron temperature. Subsequently, T_e decreases as does the photoelectron heating rate due to attenuation by the increasing flux tube content. Near 800 km the photoelectron heating is balanced principally by conduction to lower altitudes where collisional cooling to the ions and neutrals occurs. At lower altitudes the collisional cooling acts directly. Note that the ion-electron cooling rate in Figure 5 is referenced to the scale on the right in each of the panels in the top row. Comparing the local time profiles during seasons for which the H^+ fraction changes from 0.1 to 0.3, we notice that during the daytime the dominant heating and cooling terms for electrons in the topside ionosphere are not significantly affected by the ion composition. Additionally, in the winter higher neutral hydrogen densities and higher electron temperatures may contribute to higher H^+ densities.

Figure 6 shows the heating and cooling terms for O^+ as a function of local time and altitude in the same format as Figure 5. Here the additional contribution of adiabatic heating or cooling from field-aligned plasma motions (Adv) is included, in addition to those discussed earlier. At altitudes below 600 km, O^+ is heated principally by ion-electron collisions and cooled by ion-neutral collisions. By contrast, in the topside, even in the

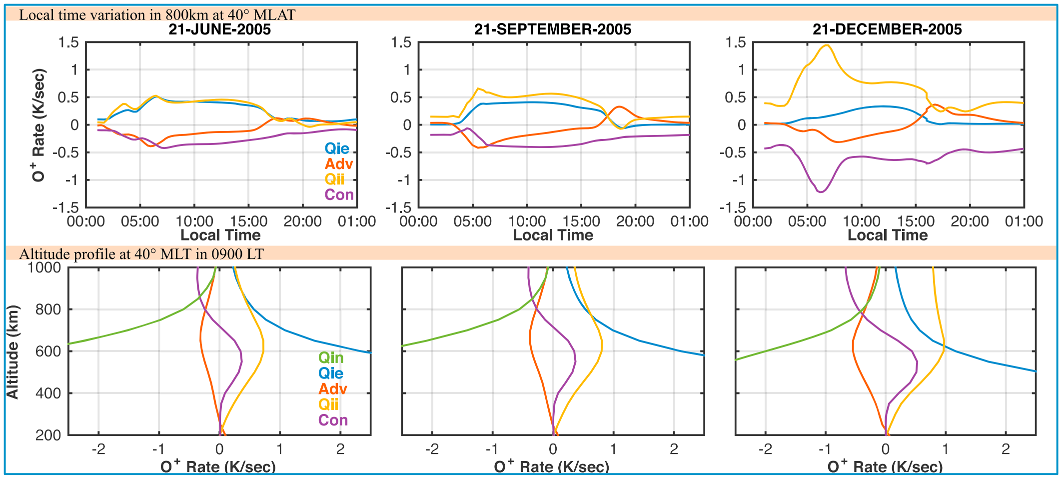

Figure 6. Model values of the major O^+ heating and cooling rates. (top row) Electron-O^+ collisional energy exchange (Q_{ie}), H^+-O^+ collisional energy exchange (Q_{ii}), thermal conduction (Con), and adiabatic heating and cooling (Adv) as a function of local time at 40° magnetic latitude in 840 km. (bottom row) Altitude profiles of the same parameters with additional O^+-neutral collisional cooling (Q_{in}) at 0900 h local time.

presence of a very small fractional population of H^+, the O^+ is heated by collisions with both electrons and light ions and cools by conducting to the region below. The altitude at which conduction and collisions with the neutral gas contribute equally to the cooling of O^+ is dependent on the neutral density profile, which we have adjusted in this case to reach agreement with observations. In the topside, as the H^+ fractional content increases in moving from summer to winter, we find that the collisional heating between the H^+ and O^+ dominates the O^+ heating rate, while conduction remains the dominant cooling term independent of the H^+ fractional content.

Shown in Figure 7 are the heating and cooling terms for H^+ as a function of local time and altitude in the same format as Figure 5. In the topside near 840 km, during the daytime H^+ remains a minor ion species with a fractional content that varies between 0.1 and 0.3. We noted that at middle latitudes, H^+ in the topside ionosphere during the daytime is almost always expanding into the flux tube volume above to fill the plasmasphere. This causes adiabatic cooling to be significant at all times. The topside H^+ is usually locally heated by collisions with the electrons. However, at lower plasma density and higher H^+ content, associated with a transition from summer to winter, the H^+ in the topside may additionally be heated by conduction from

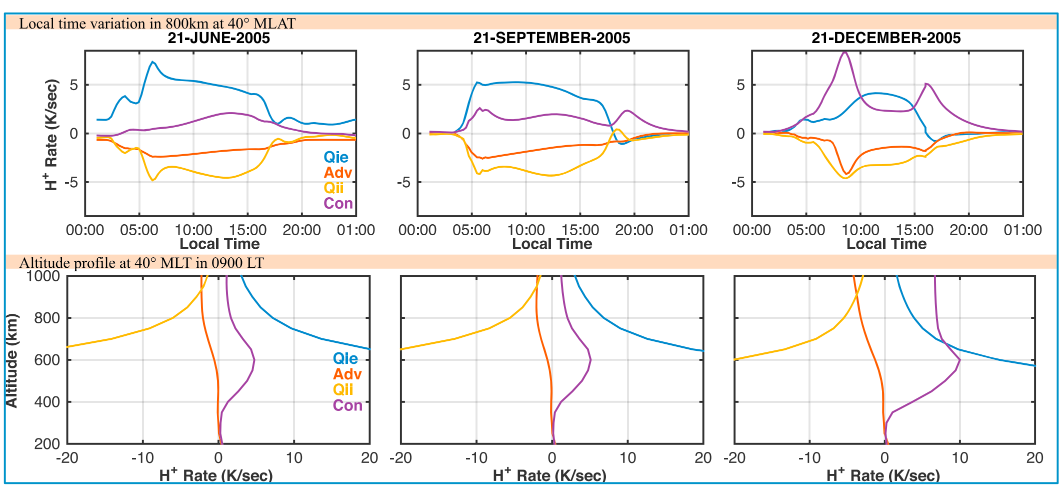

Figure 7. Model values of the major H^+ heating and cooling rates. (top row) Electron-H^+ collisional energy (Q_{ie}), H^+-O^+ collisional energy exchange (Q_{ii}), thermal conduction (Con), and adiabatic heating and cooling (Adv) as a function of local time at 40° magnetic latitude in 840 km. (bottom row) Altitude profiles of the same parameters at 0900 h local time.

the hotter H^+ at higher altitude. In all cases, the topside H^+ is cooled principally by local collisions with the heavier ions and by field-aligned motion.

In the topside ionosphere it is clear that H^+ plays the part of an intermediary for the thermal balance between electrons and O^+ ions when both species are present. Thus, in the presence of H^+, electrons are cooled through collisions with H^+ and the heat is further transferred to O^+ through collisions between H^+ and O^+. Considering the altitude profile of Figure 3, when the H^+ fraction is high T_{H+} tends to move closer to T_e, and collisional heating between O^+ and light ions can become the major heat source for O^+ in the topside as shown in Figure 6.

6. Discussion

We have successfully modeled the behavior of daytime plasma temperatures in the midlatitude topside ionosphere and provided a detailed description of the complex heat balance when both O^+ and H^+ are present. First we note that the electron thermal balance is not significantly affected by the ion composition. Electrons are heated by photoelectron fluxes transported from lower latitudes and cooled by conduction to lower altitudes. At lower altitudes the cooling occurs due to collisions with the ions and finally at the lowest altitudes by collisions with the neutral gas. For the ions, however, the basic processes differ significantly from those that are usually associated with a single ion species in the topside. This is due primarily to the inverse mass dependence that makes the energy exchange rate between the electrons and H^+ 16 times more efficient than that for O^+ with the same difference in ion and electron temperature.

Considering only O^+ in the topside, for example, this species is heated by electron collisions and cooled by conduction. At lower altitudes the ions are cooled directly by collisions with the neutral gas, and the neutral density distribution with altitude affects the altitude above which conduction dominates local collisional cooling. Adjustments to the model neutral atmosphere were made for this study to affect just such a change in order to match the observations of O^+ and electron temperature.

When H^+ is present, with fractional content greater than 10%, the O^+ heating is no longer dominated by collisions with electrons [*Dalgarno and Walker*, 1966; *Banks*, 1967]. Rather, collisions with H^+, which is efficiently heated by electron collisions and resides at higher temperatures than O^+, dominate the thermal balance for O^+. At middle latitudes in the topside, H^+ is heated by ion-electron collisions as expected. Thermal contact with the electrons increases as the H^+ fractional content increases, and this also allows conduction from above to become an important heat source for H^+ in the topside. H^+ is cooled principally by collisions with O^+. However, with increasing altitude, as H^+ becomes a major species, heat conduction to lower altitudes becomes the major cooling mechanism. The continuous outflow of H^+ into the plasmasphere during the daytime may also be a significant cooling source in the topside at middle latitudes.

7. Summary

The SAMI2 model captures the major mechanisms that control the heat flow in the topside ionosphere at middle latitudes. While it is not our purpose to quantitatively reproduce specific observations, the model plasma temperatures, as functions of plasma density, can be aligned with observations by adjusting the vertical distribution of the neutral gases. The model results confirm observations, during the daytime at middle latitudes when both O^+ and H^+ are present, that $T_{H+} > T_{O+}$ and that T_{O+} increases as the fractional content of H^+ increases at a fixed density. The model also reveals features of the heat balance in the topside when both O^+ and H^+ are present, that are different from the balance that exists when either ion is present alone.

In the most fundamental of terms we find that in the topside at middle latitudes any major species, O^+ or H^+, is heated by electron collisions and cooled by conduction. However, in the intervening altitude region where both O^+ and H^+ are present, O^+ is heated by collisions with H^+ and cooled by conduction, while H^+ is heated by collisions with electrons and cooled by collisions with O^+. The heat balance between the H^+ and O^+ always keeps the H^+ at a temperature higher than the O^+, with differences as large as 1000 K dependent on the solar zenith angle and the fractional contribution of H^+ and O^+ to the total plasma density. Further observations of both T_{H+} and T_{O+} would permit the role of heat exchange between these two species to be assessed in the topside ionosphere in more dynamic situations where field-aligned motions are important.

Acknowledgments
This work is supported by NASA Grant NNX10AT02G to the University of Texas at Dallas. The solar ionizing flux ($F_{10.7}$) are available via the Space Physics Data Facility OMNIWeb interface. The link to this database is http://omniweb.gsfc.nasa.gov. The DMSP plasma data were obtained from the William B. Hanson Center for Space Sciences at the University of Texas at Dallas. The data before 2005 are available at http://cindispace.utdallas.edu/DMSP/dmsp_data_at_utdallas.html, and the data after 2005 can be requested from Marc Hairston (hairston@utdallas.edu). The authors thank Robin Coley, Marc Hairston, and Bob Power for their use. This work uses the SAMI2 ionosphere model written and developed by the Naval Research Laboratory. We thank J. Klenzing for discussions related to adjustment of the neutral model in SAMI2.

References

Bailey, G. J., Y. Z. Su, and K.-I. Oyama (2000), Yearly variations in the low-latitude topside ionosphere, *Ann. Geophys.*, *18*, 789–798, doi:10.1007/s00585-000-0789-0.

Banks, P. M. (1967), Ion temperature in the upper atmosphere, *J. Geophys. Res.*, *72*(13), 3365–3385, doi:10.1029/JZ072i013p03365.

Banks, P. M., and G. Kockarts (1973), *Aeronomy*, pp. 287–304, Academic Press, San Diego, Calif.

Bilitza, D. (1975), Models for the relationship between electron density and temperature in the upper ionosphere, *J. Atmos. Terr. Phys.*, *37*(9), 1219–1222, doi:10.1016/0021-9169(75)90193-2.

Bilitza, D., V. Truhlik, P. Richards, T. Abe, and L. Triskova (2007), Solar cycle variations of mid-latitude electron density and temperature: Satellite measurements and model calculations, *Adv. Space Res.*, *39*, 779–789.

Brace, L. H., and R. F. Theis (1978), An empirical model of the interrelationship of electron temperature and density in the daytime thermosphere at solar minimum, *Geophys. Res. Lett.*, *5*, 275–278, doi:10.1029/GL005i004p00275.

Burrell, A. G., and R. A. Heelis (2012), The influence of hemispheric asymmetries on field-aligned ion drifts at the geomagnetic equator, *Geophys. Res. Lett.*, *39*, L19101, doi:10.1029/2012GL053637.

Chao, C. K., S.-Y. Su, J. D. Huba, and K.-I. Oyama (2010), Modeling the presunrise plasma heating in the low- to midlatitude topside ionospheres, *J. Geophys. Res.*, *115*, A09304, doi:10.1029/2009JA014923.

Chapman, S. (1931), Absorption and dissociative or ionising effects of monochromatic radiation in an atmosphere on a rotating Earth, *Proc. Phys. Soc., London*, *43*, 1047–1055.

Chen, C. H., J. D. Huba, A. Saito, C. H. Lin, and J. Y. Liu (2011), Theoretical study of the ionospheric Weddell Sea Anomaly using SAMI2, *J. Geophys. Res.*, *116*, A04305, doi:10.1029/2010JA015573.

Dalgarno, A., and J. C. G. Walker (1966), Ion temperatures in the topside ionosphere, *Planet. Space Sci.*, *15*, 200–203.

Fallen, C. T., and B. J. Watkins (2013), Diurnal and seasonal variation of electron heat flux measured with the Poker Flat Incoherent-Scatter Radar, *J. Geophys. Res. Space Physics*, *118*, 5327–5332, doi:10.1002/jgra.50485.

Hedin, A. E., et al. (1996), Empirical wind model for the upper, middle, and lower atmosphere, *J. Atmos. Terr. Phys.*, *58*, 1421–1447, doi:10.1016/0021-9169(95)00122-0.

Heelis, R. A. and W. B. Hanson (1998), Measurements of thermal ion drift velocity and temperature using planar sensors, in *Measurement Techniques in Space Plasmas: Particles*, edited by R. F. Pfaff, J. E. Borovsky, and D. T. Young, pp. 61–71, AGU, Washington, D. C., doi: 10.1029/GM102p0061.

Hsu, C.-T., and R. A. Heelis (2017), Daytime ion and electron temperatures in the topside ionosphere at middle latitudes, *J. Geophys. Res. Space Physics*, *122*, 2202–2209, doi:10.1002/2016JA023599.

Huba, J. D., G. Joyce, and J. A. Fedder (2000), Sami2 is Another Model of the Ionosphere (SAMI2): A new low-latitude ionosphere model, *J. Geophys. Res.*, *105*(A10), 23,035–23,053, doi:10.1029/2000JA000035.

Hysell, D. L., M. A. Milla, F. S. Rodrigues, R. H. Varney, and J. D. Huba (2015), Topside equatorial ionospheric density, temperature, and composition under equinox, low solar flux conditions, *J. Geophys. Res. Space Physics*, *120*, 3899–3912, doi:10.1002/2015JA021168.

Kakinami, Y., S. Watanabe, J.-Y. Liu, and N. Balan (2011), Correlation between electron density and temperature in the topside ionosphere, *J. Geophys. Res.*, *116*, A12331, doi:10.1029/2011JA016905.

Kakinami, Y., S. Watanabe, M.-y. Yamamoto, and C.-K. Chao (2014), Correlations between ion density and temperature in the topside ionosphere measured by ROCSAT-1, *J. Geophys. Res. Space Physics*, *119*, 9207–9215, doi:10.1002/2014JA020302.

Klenzing, J., A. G. Burrell, R. A. Heelis, J. D. Huba, R. F. Pfaff, and F. Simões (2013), Exploring the role of ionospheric drivers during the extreme solar minimum of 2008, *Ann. Geophys.*, *31*, 2147–2156, doi:10.5194/angeo-31-2147-2013.

Klimenko, M., V. V. Klimenko, and V. V. Bryukhanov (2008), Numerical modeling of the light ion trough and heat balance of the topside ionosphere in quiet geomagnetic conditions, *J. Atmos. Sol. Terr. Phys.*, *70*(17), 2144–2158, doi:10.1016/j.jastp.2008.08.001.

Millward, G. H., R. J. Moett, S. Quegan, and T. J. Fuller-Rowell (1996), A coupled thermosphere-ionosphere-plasmasphere model (CTIP), in *Solar Terrestrial Energy Program (STEP) Handbook of Ionospheric Models*, edited by R. W. Schunk, pp. 239–279, Utah State Univ., Logan.

Picone, J. M., A. E. Hedin, D. P. Drob, and A. C. Aikin (2002), NRLMSISE-00 empirical model of the atmosphere: Statistical comparisons and scientific issues, *J. Geophys. Res.*, *107*(A12), 1468, doi:10.1029/2002JA009430.

Qian, L., A. G. Burns, B. A. Emery, B. Foster, G. Lu, A. Maute, A. D. Richmond, R. G. Roble, S. C. Solomon, and W. Wang (2014), The NCAR TIE-GCM: A community model of the coupled thermosphere/ionosphere system, in *Modeling the Ionosphere-Thermosphere System*, *Geophys. Monogr. Ser.*, edited by J. Huba, R. Schunk, and G. Khazanov, pp. 73–83, John Wiley, Chichester, U. K., doi:10.1002/9781118704417.

Richards, P. G., J. A. Fennelly, and D. G. Torr (1994), EUVAC: A solar EUV flux model for aeronomic calculations, *J. Geophys. Res.*, *99*(A5), 8981–8992, doi:10.1029/94JA00518.

Richards, P. G., M. J. Nicolls, C. J. Heinselman, J. J. Sojka, J. M. Holt, and R. R. Meier (2009), Measured and modeled ionospheric densities, temperatures, and winds during the international polar year, *J. Geophys. Res.*, *114*, A12317, doi:10.1029/2009JA014625.

Richmond, A. D., E. C. Ridley, and R. G. Roble (1992), A thermosphere/ionosphere general circulation model with coupled electrodynamics, *Geophys. Res. Lett.*, *19*, 601–604.

Schunk, R. W., and A. F. Nagy (1978), Electron temperatures in the *F* region of the ionosphere: Theory and observations, *Rev. Geophys.*, *16*(3), 355–399, doi:10.1029/RG016i003p00355.

Su, Y. Z., G. J. Bailey, and K.-I. Oyama (1998), Annual and seasonal variations in the low-latitude topside ionosphere, *Ann. Geophys.*, *16*, 974–985, doi:10.1007/s00585-998-0974-0.

Titheridge, J. E. (1998), Temperatures in the upper ionosphere and plasmasphere, *J. Geophys. Res.*, *103*(A2), 2261–2277, doi:10.1029/97JA03031.

Varney, R. H., W. E. Swartz, D. L. Hysell, and J. D. Huba (2012), SAMI2-PE: A model of the ionosphere including multistream interhemispheric photoelectron transport, *J. Geophys. Res.*, *117*, A06322, doi:10.1029/2011JA017280.

Wang, W., A. G. Burns, and T. L. Killeen (2006), A numerical study of the response of ionospheric electron temperature to geomagnetic activity, *J. Geophys. Res.*, *111*, A11301, doi:10.1029/2006JA011698.

Wu, T.-W., J. D. Huba, G. Joyce, and P. A. Bernhardt (2012), Modeling Arecibo conjugate heating effects with SAMI2, *Geophys. Res. Lett.*, *39*, L07103, doi:10.1029/2012GL051311.

Zhang, S.-R., J. M. Holt, A. M. Zalucha, and C. Amory-Mazaudier (2004), Midlatitude ionospheric plasma temperature climatology and empirical model based on Saint Santin incoherent scatter radar data from 1966 to 1987, *J. Geophys. Res.*, *109*, A11311, doi:10.1029/2004JA010709.